Monthly Notices
of the
ROYAL ASTRONOMICAL SOCIETY

MNRAS **437,** 1155–1170 (2014)
Advance Access publication 2013 November 26

doi:10.1093/mnras/stt1913

Interaction effects on galaxy pairs with Gemini/GMOS- I: Electron density

A. C. Krabbe,[1]★ D. A. Rosa,[1] O. L. Dors Jr,[1] M. G. Pastoriza,[2] C. Winge,[3] G. F. Hägele,[4,5] M. V. Cardaci[4,5] and I. Rodrigues[1]

[1]*Universidade do Vale do Paraíba, Av. Shishima Hifumi, 2911, Cep 12244-000, São José dos Campos, SP, Brazil*
[2]*Instituto de Física, Universidade Federal do Rio Grande do Sul, Av. Bento Gonçalves, 9500, Cep 91359-050, Porto Alegre, RS, Brazil*
[3]*Gemini Observatory, c/o AURA Inc., Casilla 603, La Serena, Chile*
[4]*Instituto de Astrofísica de La Plata (CONICET La Plata–UNLP), Argentina*
[5]*Facultad de Ciencias Astronómicas y Geofísicas, Universidad Nacional de La Plata, Paseo del Bosque s/n, 1900 La Plata, Argentina*

Accepted 2013 October 4. Received 2013 September 16; in original form 2013 May 13

ABSTRACT

We present an observational study about the impacts of the interactions on the electron density of H II regions located in seven systems of interacting galaxies. The data consist of long-slit spectra in the range 4400–7300 Å, obtained with the Gemini Multi-Object Spectrograph at Gemini South (GMOS-S). The electron density was determined using the ratio of emission lines [S II] λ6716/λ6731. Our results indicate that the electron density estimates obtained of H II regions from our sample of interacting galaxies are systematically higher than those derived for isolated galaxies. The mean electron density values of interacting galaxies are in the range of $N_e = 24$–$532\,cm^{-3}$, while those obtained for isolated galaxies are in the range of $N_e = 40$–$137\,cm^{-3}$. Comparing the observed emission lines with predictions of photoionization models, we verified that almost all the H II regions of the galaxies AM 1054A, AM 2058B and AM 2306B have emission lines excited by shock gas. For the remaining galaxies, only few H II regions have emission lines excited by shocks, such as in AM 2322B (one point) and AM 2322A (four points). No correlation is obtained between the presence of shocks and electron densities. Indeed, the highest electron density values found in our sample do not belong to the objects with gas shock excitation. We emphasize the importance of considering these quantities especially when the metallicity is derived for these types of systems.

Key words: galaxies: general – galaxies: interactions – galaxies: ISM.

1 INTRODUCTION

The study of physical processes involved in galaxy collisions and mergers in the local Universe is fundamental to understand the formation and evolution of these objects, providing important constraints in simulations of the universe at large scale.

In particular, the chemical abundance is highly modified in interacting/merging galaxies. Kewley et al. (2010) presented a systematic investigation about metallicity gradients in close pairs of galaxies. These authors determined the oxygen abundance (generally used as a tracer of the metallicity *Z*) along the disc of eight galaxies in close pairs and found metallicity gradients shallower than the ones in isolated galaxies. Similar results have been reached by Krabbe et al. (2011, 2008), who built spatial profiles of oxygen abundance of the gaseous phase of the galaxy pairs AM 2306-721 and AM 2322-2821. This flattening in the oxygen abundance gradient reflects the effects of gas redistribution along the galaxy disc due to metal-poor inflow of gas from the outskirts of the centre of interacting galaxies (Rupke, Kewley & Chien 2010).

The large-scale gas motion created by the interaction induces high star formation rate (SFR) and galactic-scale outflows (Veilleux, Cecil & Bland-Hawthorn 2005), producing shock excitation in star-forming regions, such as reported in recent studies of luminous infrared galaxies by Soto & Martin (2012), Rich et al. (2012) and Rich, Kelley & Dopita (2011). In particular, Rich et al. (2011), through integral field spectroscopic data of the luminous infrared galaxies IC 1623 and NGC 3256, showed that broad line profiles are often associated with gas shock excitation in H II regions located in mergers. Similar results were also found by Newman et al. (2012) for the clumpy star-forming galaxy ZC 406690 (see also Soto et al. 2012). These authors pointed out that the broad emission likely originates from large-scale outflows with high mass rates from individual star-forming regions. The changes in galaxies that experience an encounter seem to have a relation with the separation among the objects interacting, such as showed by Scudder et al. (2012).

★ E-mail: angela.krabbe@gmail.com

These authors, using spectroscopy data of a large sample of objects with a close companion taken from the Sloan Digital Sky Survey Data Release, found that the metallicity gradient and the SFR are correlated with the separation of the galaxy pairs analysed, in the sense that the gradients are flatter and the SFR are higher at smaller separations.

Despite recent efforts to probe the properties of interacting galaxies, the electron densities of star-forming regions have been poorly determined in these systems, as well as its correlation with other quantities (e.g. *Z*, SFR). In galaxy discs of interacting galaxies, where gas motions and gas excited by shock are present, high electron density is expected and can be used as a signature of the presence of these motions and shocks. In fact, Puech et al. (2006), in a study about galaxy interaction, mapped electron densities in six distant galaxies ($z \sim 0.55$) and found that the highest electron density values observed could be associated with the collision between molecular clouds of the interstellar medium and gas inflow/outflow events. These authors derived electron density values lower than 400 cm^{-3}, typical of classical H II regions (Castañeda, Vílchez & Copetti 1992; Copetti et al. 2000). However, Puech et al. (2006) used as a sensor the [O II] λ3729/λ3727 ratio, which underestimates the electron density in relation to determinations via other line ratios (Copetti & Writzl 2002). Most of oxygen determinations of the gas phase in interacting galaxies (e.g. Krabbe et al. 2008, 2011; Kewley et al. 2010; Rich et al. 2011, 2012; Scudder et al. 2012) are based on theoretical models that consider low electron density values of 10–200 cm^{-3} (Dopita et al. 2000; Kewley & Dopita 2002; Dors et al. 2011; Krabbe et al. 2011). If the electron density values considerably differ from those considered in the models, the oxygen abundance estimations will be doubtful. In fact, Oey & Kennicutt (1993) showed that systematic variations in the nebular density introduce significant uncertainties into the abundances obtained using methods based on strong emission lines. They found that differences between 10 and 200 cm^{-3}, a typical range for the electron density derived in giant H II regions (e.g. Kennicutt 1984; O'dell & Castañeda 1984; Castañeda et al. 1992; Copetti et al. 2000), reflect variations up to 0.5 dex in oxygen abundances, mainly for the high-metallicity regime. These variations can increase even more when higher electron density values, such as the ones found in star-forming clumps (e.g. 300–1800 cm^{-3}; Newman et al. 2012), are considered in abundance determinations.

In this paper, we used long-slit spectroscopic data of a sample of seven pair galaxies to verify the effects of the interaction on the electron density in these systems. This work is organized as follows. In Section 2, we summarize the observations and data reduction. In Section 3, the method to compute the electron density is described. Results and discussion are presented in Sections 4 and 5, respectively. The conclusions of the outcomes are given in Section 6.

2 OBSERVATIONS AND DATA REDUCTION

We have selected several systems from Ferreiro & Pastoriza (2004) to study the effects of the kinematics, stellar population, gradient abundances and electron densities of interacting galaxies. The first results of this programme were presented for AM2306-721 (Krabbe et al. 2008) and AM2322-821 (Krabbe et al. 2011). Table 1 summarizes the main characteristics of the systems: identification, morphology, position, radial velocity, apparent *B* magnitude and other designations.

Long-slit spectroscopic data were obtained in May, June and July 2006 and 2007, and July 2008 with the Gemini Multi-Object Spectrograph at Gemini South (GMOS-S) attached to the 8 m Gemini South telescope, Chile, as part of the poor weather programmes GS-2006A-DD-6, GS-2007A-Q-76 and GS-2008A-Q-206. Spectra in the range 4400–7300 Å were acquired with the B600 grating, and 1 arcsec slit width, assuming a compromise between spectral resolution (5.5 Å), spectral coverage and slit losses (due to the Image Quality = ANY constraint). The frames were binned on-chip by 4 and 2 pixels in the spatial and spectra directions, respectively, resulting in a spatial scale of 0.288 arcsec pixel^{-1} and dispersion of 0.9 Å pixel^{-1}.

Spectra were taken at different position angles on the sky, with the goal of observing the nucleus and the brightest regions of the galaxies. The exposure time on each single frame was limited to 700 s to minimize the effects of cosmic rays, with multiple frames being obtained for each slit position to achieve a suitable signal. The slit positions for each system are shown in Fig. 1, superimposed on the GMOS-S r' acquisition images. Table 2 gives the journal

Table 1. Galaxy sample.

ID	Morphology	α(2000) ($^{\mathrm{h}}$ $^{\mathrm{m}}$ $^{\mathrm{s}}$)	δ(2000) ($^{\circ}$ $'$ $''$)	cz (km s^{-1})	m_{B} (mag)	Others' names
AM 1054-325	Sm [2]	10 56 58.2	−33 09 52.0	3 788 [10]	14.55 [2]	ESO 376-IG 027
	Sa [5]	10 57 04.2	−33 09 21.0	3 850 [5]	15.41 [8]	ESO 376- G 028
AM 1219-430	Sm [6]	12 21 57.3	−43 20 05.0	6 957 [3]	14.30 [7]	ESO 267-IG 041
	S? [6]	12 22 04.0	−43 20 21.0	6 879 [3]	–	FAIRALL 0157
AM 1256-433	E [3]	12 58 50.9	−43 52 30.0	9 215 [3]	14.75 [8]	ESO 269-IG 022 NED01
	E [3]	12 58 50.6	−43 52 53.0	9 183 [3]	16.17 [8]	ESO 269-IG 022 NED02
	SBC [3]	12 58 57.6	−43 50 11.0	9 014 [3]	16.41 [1]	ESO 269-IG 023 NED01
AM 2058-381	Sbc [6]	21 01 39.1	−38 04 59.0	12 383 [3]	14.91 [1]	ESO 341- G 030
	?	21 01 39.9	−38 05 53.0	12 460 [3]	16.24 [1]	ESO 341- G 030 NOTES01
AM 2229-735	SO? [3]	22 33 43.7	−73 40 47.0	17 535 [3]	15.98 [1]	AM 2229-735 NED01
	?	22 33 48.3	−73 40 56.0	17 342 [3]	17.36 [1]	AM 2229-735 NED02
AM 2306-721	SAB(r)c	23 09 39.3	−71 01 34.0	8 919 [4]	14.07 [1]	ESO 077- G 003
	?	23 09 44.5	−72 00 04.0	8 669 [4]	14.47 [1]	ESO 077-IG 004
AM 2322-821	SA(r)c	23 26 27.6	−81 54 42.0	3 680 [3]	13.35 [1]	ESO 012- G 001, NGC 7637
	?	23 25 55.4	−81 52 41.0	3 376 [4]	15.41 [1]	ESO 012- G 001 NOTES01

References: [1] Ferreiro & Pastoriza (2004); [2] Weilbacher et al. (2000); [3] Donzelli & Pastoriza (1997); [4] Krabbe et al. (2011); [5] Lauberts (1982)); [6] Paturel et al. (2003); [7] de Vaucouleurs et al. (1991); [8] Lauberts & Valentijn (1989); [9] Huchra et al. (2012); [10] Jones et al. (2009).

Conventions: α, δ – equatorial coordinates.

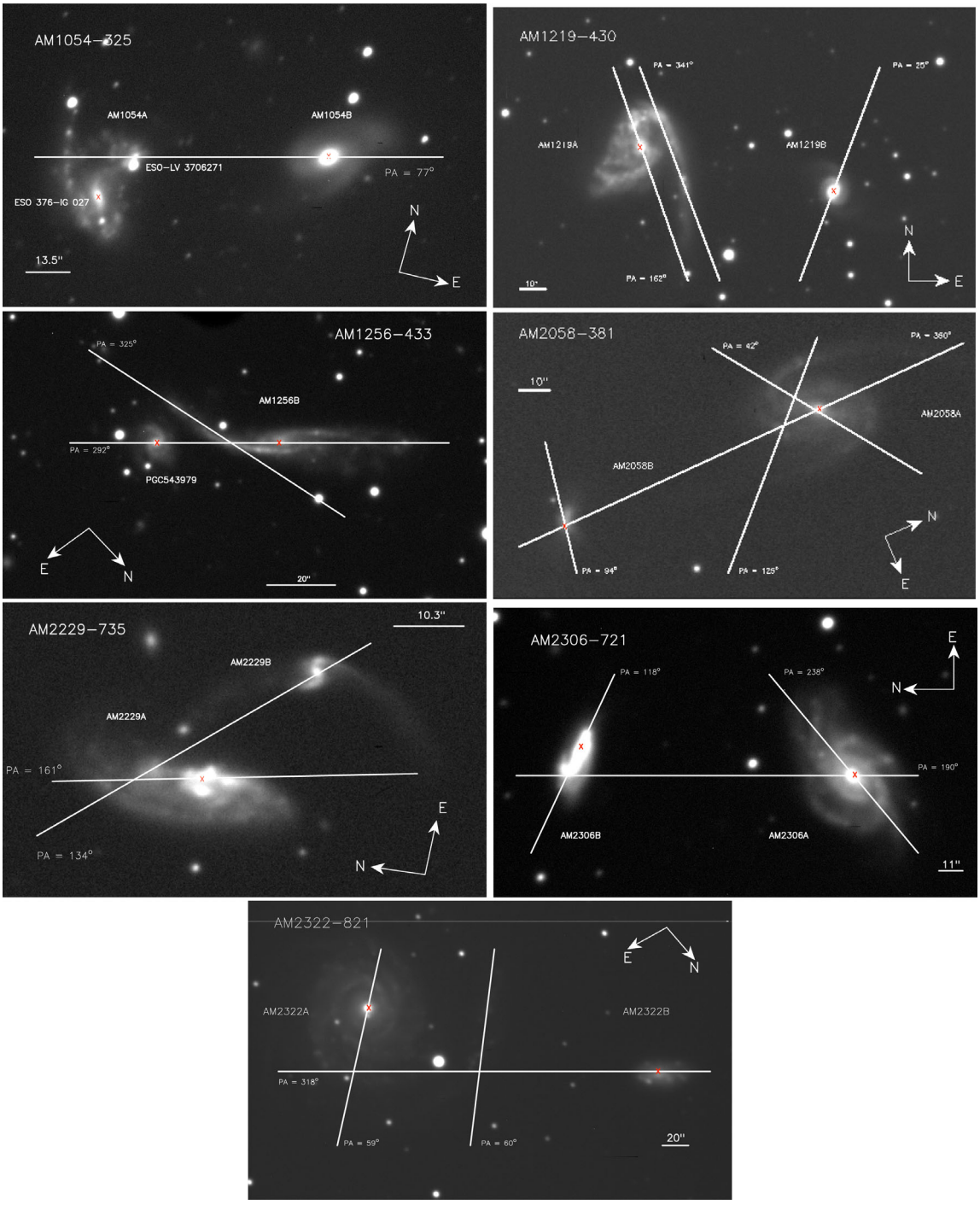

Figure 1. The slit positions for each system are shown superimposed on the GMOS-S r' acquisition image.

of observations. Conditions during the observing runs were not photometric, with thin cirrus and image quality in the range 0.6–1.7 arcsec (as measured from stars in the acquisition images taken just prior to the spectroscopic observations).

The spectroscopic data reduction was carried out using the GEMINI.GMOS package and generic IRAF[1] tasks. We followed the standard procedure: (1) the data were bias subtracted and flat-fielded; (2) the wavelength calibration was established from the Cu–Ar arc frames with typical residuals of 0.2 Å and applied to the object frames; (3) the individual spectra of the same slit positions and wavelength range were averaged with cosmic ray rejection; (4) the object frames were sky subtracted interactively using the GSSKYSUB task, which uses a background sample of off-object areas to fit a function to the specified rows, and this fit was then subtracted from the column of each spectrum; (5) the spectra were relative flux calibrated using observations of a flux standard star taken with the same set up as the science observations; (6) finally,

[1] Image Reduction and Analysis Facility, distributed by National Optical Astronomy Observatory, operated by AURA, Inc., under agreement with NSF.

Table 2. Journal of observations.

Object	Date	Exposure time (s)	PA (°)	Δ λ (Å)
AM 1054-325	2007-06-21	4 × 600	77	4280–7130
AM 1219-430	2007-06-06	4 × 600	25	4280–7130
	2007-05-26	4 × 600	162	4280–7130
	2007-06-22	4 × 600	341	4280–7130
AM 1256-433	2007-07-06	4 × 600	292	4280–7130
	2007-06-21	4 × 600	325	4280–7130
AM 2058-381	2006-05-20	4 × 600	42	4351–7213
	2007-05-26	4 × 600	94	4351–7213
	2007-05-24	4 × 600	125	4351–7213
	2007-05-30	4 × 600	350	4351–7213
AM 2229-735	2006-07-20	6 × 600	134	4390–7250
	2006-07-16	6 × 600	161	4390–7250
AM 2306-721	2006-06-20	4 × 600	118	4280–7130
	2006-06-20	4 × 600	190	4280–7130
	2006-06-20	4 × 600	238	4280–7130
AM 2322-821	2006-07-01	3 × 700	59	4280–7130
	2008-07-27	6 × 600	60	4280–7130
	2006-06-30	6 × 600	318	4280–7130

one-dimensional spectra were extracted from the two-dimensional spectra by summing over four rows along the spatial direction. Each spectrum, therefore, comprises the flux contained in an aperture of 1 arcsec × 1.152 arcsec.

The intensities of the Hβ, [O III] λ5007, [O I] λ6300, Hα, [N II] λ6584 and [S II] λλ6716, 6731 emission lines were measured using a single Gaussian line profile fitting on the spectra. We used the IRAF SPLOT routine to fit the lines, with the associated error being given as $\sigma^2 = \sigma^2_{\rm cont} + \sigma^2_{\rm line}$, where $\sigma_{\rm cont}$ and $\sigma_{\rm line}$ are the continuum rms and the Poisson error of the line flux, respectively. Furthermore, we considered only measurements whose continuum around λ6700 Å reaches a signal-to-noise S/N ≥ 8. The emission line intensities were not corrected for the interstellar extinction, because it is negligible due to the small separation between the [S II] λ6716 and λ6731 emission lines.

3 DETERMINATION OF THE ELECTRON DENSITY

The electron density $N_{\rm e}$ was derived from the [S II] λ6716/λ6731 emission line intensity ratio by solving numerically the equilibrium equation for an n-level atom approximation using the TEMDEN routine of the NEBULAR package of the STSDAS/IRAF, assuming an electron temperature of 10 000 K, because temperature sensitive emission lines were unobservable in our sample.

The references for the collision strengths, transition probabilities and energy levels are Ramsbottom, Bell & Stafford (1996), Verner, Verner & Ferland (1987), Keenan et al. (1993) and Bowen (1960). There are two main sources of errors in the determination of electron densities. One is the dependence of the $N_{\rm e}$ on the electron temperature $T_{\rm e}$ assumed. However, this dependence is weak in the range of temperatures usually found in galactic H II regions (e.g. Copetti et al. 2000). We adopted a mean electron temperature of 10 000 K as a representative value, because it is a typical electron temperature value for these kinds of objects and there are no estimations for our sample. The other main source of error is the saturation of the line ratio for both low and high values of the electron density, which makes the [S II] λ6716/λ6731 ratio a reliable sensor of the electron density in the range of $2.45 < \log N_{\rm e}\ ({\rm cm}^{-3}) < 3.85$ (Stanghellini & Kaler 1989).

4 RESULTS

Fig. 2 shows a sample of the spectra of some H II regions of the galaxies around the [S II] λλ6716, 6731 emission lines. The profiles of log ([O I] λ6300/Hα), [S II] λ6716/λ6731 ratio and $N_{\rm e}$ as a function of the galactocentric radius for the galaxies are shown in Figs 3–14. The intensity of log ([O I] λ6300/Hα) was plotted only for the apertures for which the electron density determination was possible. The galactocentric radius is not corrected by galaxy inclination. In Fig. 1, the adopted centre of each galaxy is marked with a red cross. Table 3 presents some statistics of the [S II] λ6716/λ6731 ratio and electron density measurements, including the number N of distinct nebular areas, the mean, the median, the maximum and minimum, and the standard deviation σ. The results for each system are presented separately.

4.1 AM 1054-325

This system is composed of a peculiar spiral with disturbed arms (hereafter AM 1054A) and a spiral-like object (hereafter AM 1054B). AM 1054A contains very luminous H II regions along their galactic disc. As can be seen in Fig. 1, AM 1054A seems to have two nuclei. According to the measurements obtained from Weilbacher et al. (2000), the 'main' nucleus of this galaxy (ESO 376-IG 027) is the reddest [$(B - V) = 0.52$], while the other (ESO-LV 3760271) has the blue colours of a strong starburst

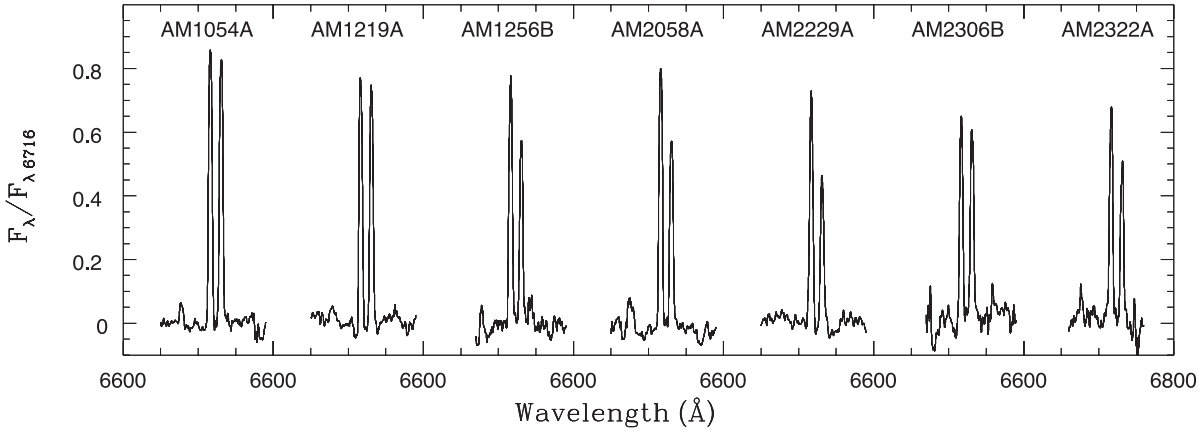

Figure 2. A sample of spectra in the range of 6600–6800 Å from areas of different galaxies. The flux scale was normalized to the peak of [S II] λ6716.

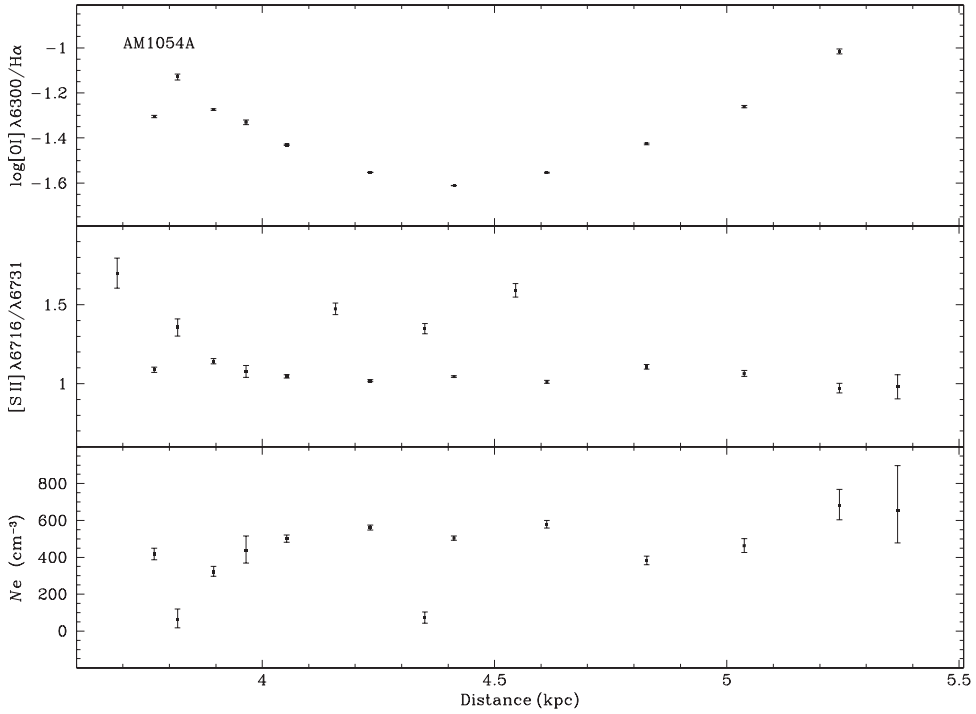

Figure 3. AM 1054-325. log ([O I λ6300/Hα) ratio, [S II] λ6716/λ6731 ratio and N_e as a function of the galactocentric radius for AM 1054A.

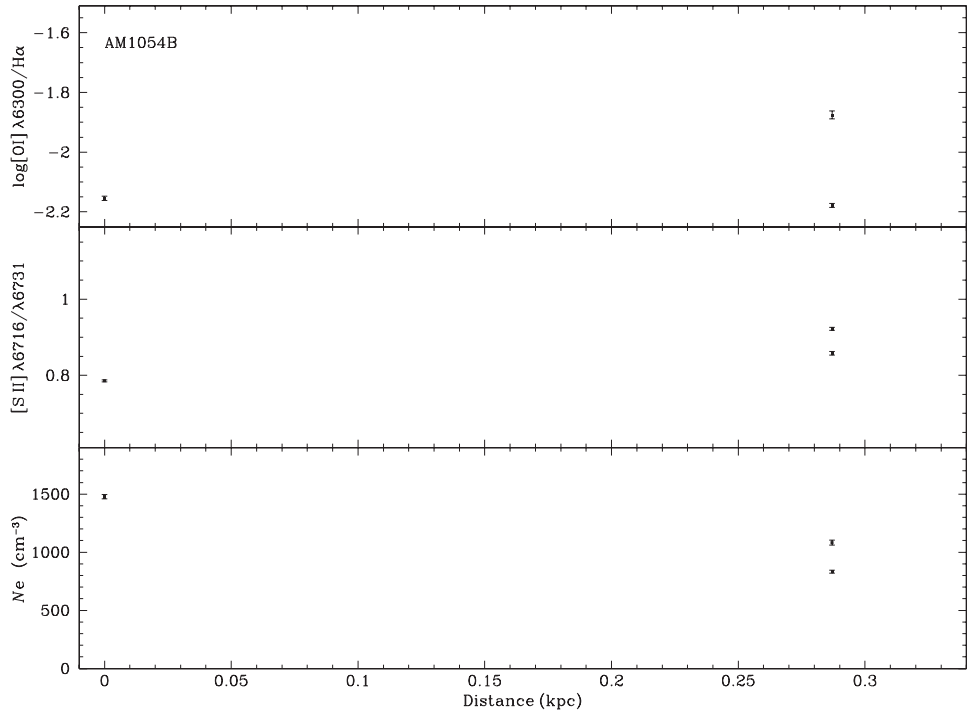

Figure 4. Same as Fig. 3, but for AM 1054B.

$[(B - V) = 0.21]$. Names of both nuclei are marked in Fig. 1. The measured radial velocity is 3788 km s^{-1} (Jones et al. 2009) and 3853 km s^{-1} (Sekiguchi & Wolstencroft 1993) for ESO 376-IG 027 and ESO-LV 3760271, respectively. Therefore, the small difference found between their radial velocities together with the perturbed morphology of the galaxy seems to indicate that these objects are gravitationally bound.

For AM 1054A, the electron density values estimated from the [S II] λ6716/λ6731 ratio (see Fig. 3) present variations of relatively high amplitude along the radius of the galaxy, with the minimum value of $N_e = 65\,\mathrm{cm}^{-3}$ and the maximum of $N_e = 681\,\mathrm{cm}^{-3}$. We found a mean density of $N_e = 434 \pm 53\,\mathrm{cm}^{-3}$. In this galaxy, the slit position is cutting a bright star-forming region, but does not cross the nucleus of the galaxy. For AM1054B, only few apertures

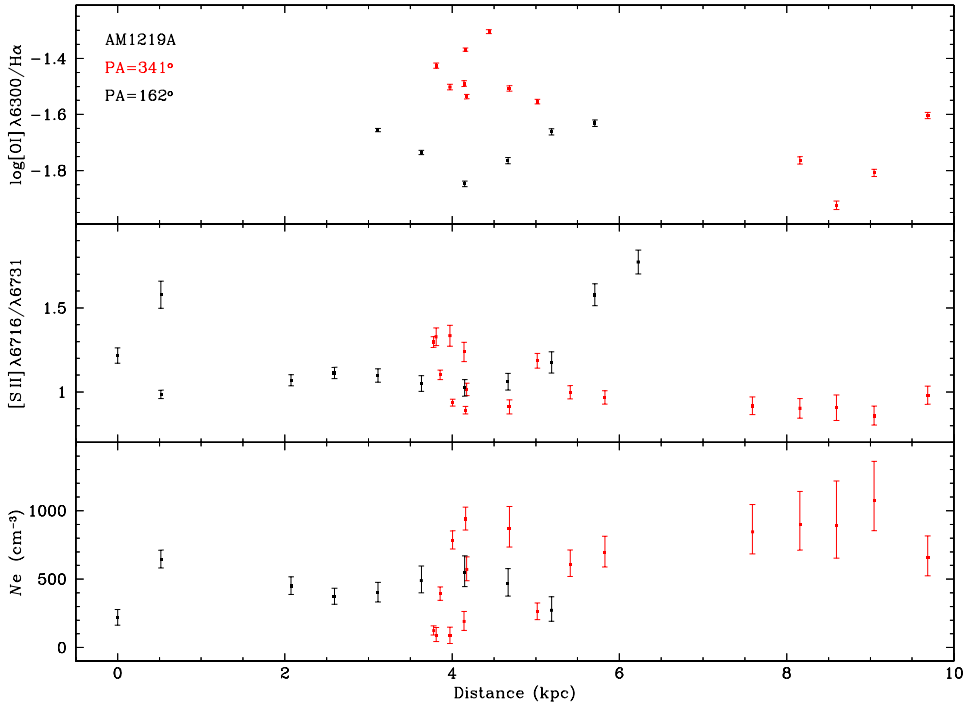

Figure 5. Same as Fig. 3, but for AM 1219A.

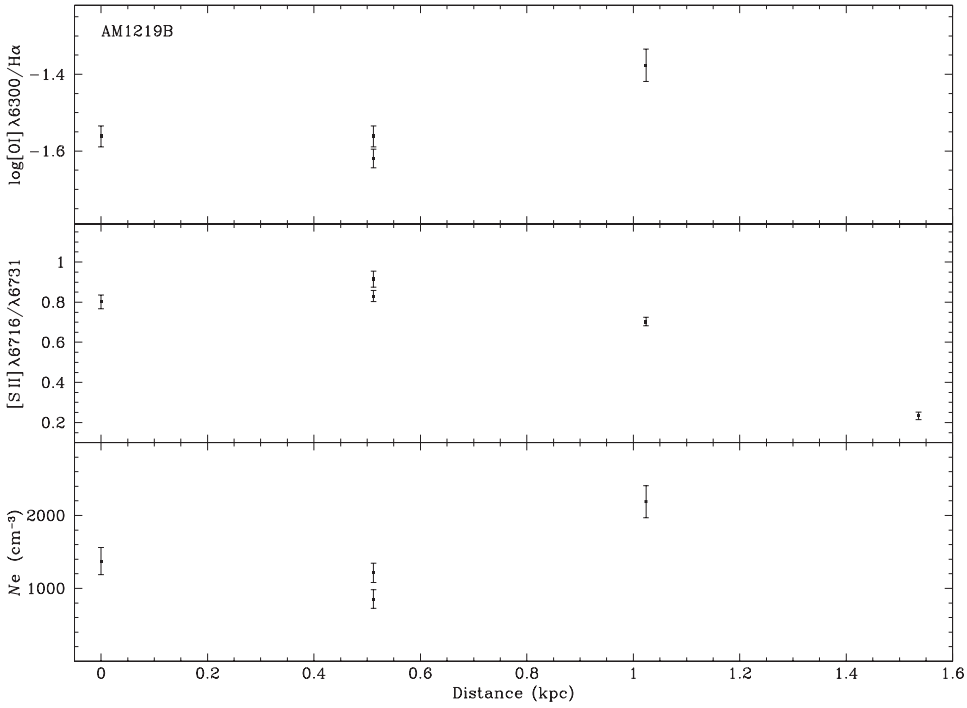

Figure 6. Same as Fig. 3, but for AM 1219B.

had the [S II] λλ6716, 6731 emission lines with enough signal to be measured. A mean density of $N_e = 1\,130 \pm 187\,cm^{-3}$ was derived for this galaxy.

4.2 AM 1219-430

This pair is composed of a disturbed spiral (hereafter AM 1219A) and a smaller disc galaxy (AM 1219B). AM 1219A shows a tidal tail produced by the interaction of the galaxies, with very bright H II regions. Systemic velocities of 6957 and 6879 km s^{-1} were estimated by Donzelli & Pastoriza (1997) for AM 1219A and AM1219B, respectively.

The distribution of electron densities exhibits variations of high amplitude across the radius of the main galaxy in the range of N_e = 85–1073 cm^{-3}. We found a mean density of $N_e = 532 \pm 56\,cm^{-3}$. As in the case of AM 1054B, only for few apertures of AM 1219B the [S II] λλ6716, 6731 emission lines have enough signal to be measured. A mean density of

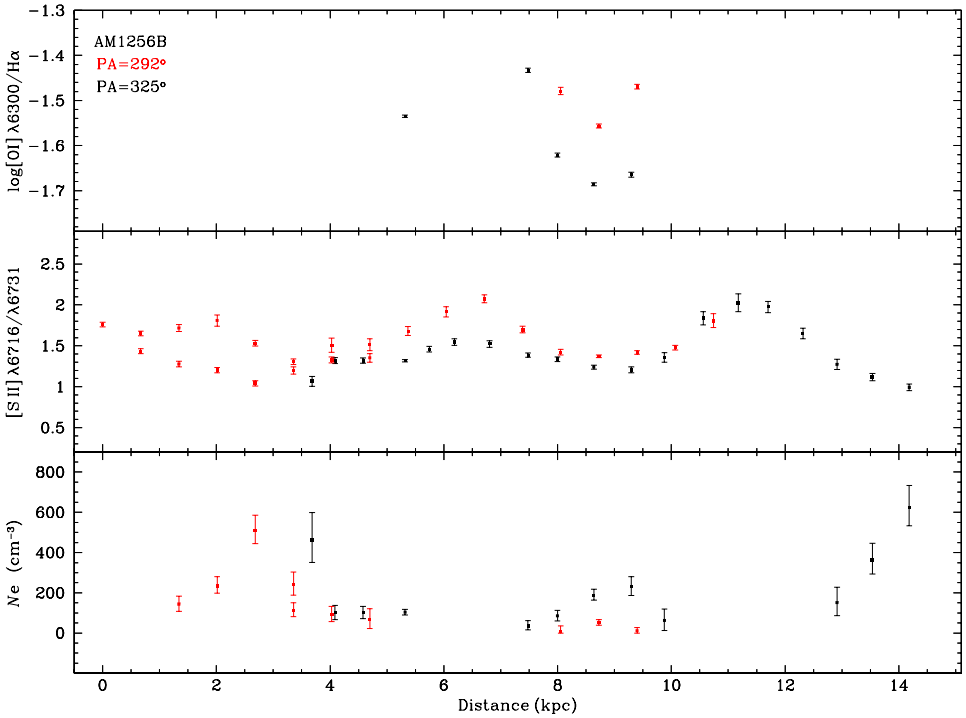

Figure 7. Same as Fig. 3, but for AM 1256B.

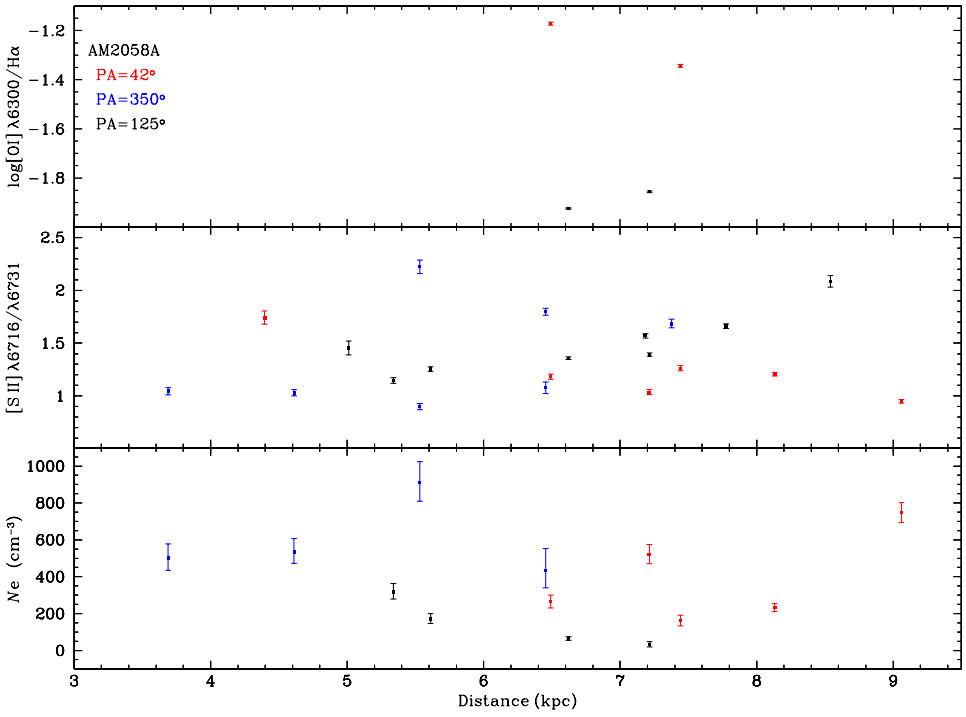

Figure 8. Same as Fig. 3, but for AM 2058A.

$N_e = 1\,408 \pm 282\,cm^{-3}$ was derived for this galaxy. Interestingly, the N_e increases towards the outskirts of this galaxy. This region is at the end of the spiral arm to the north-west.

4.3 AM 1256-433

AM 1256-433 is a system composed of three galaxies. Two are elliptical with very bright nuclei, ESO 269-IG 022 NED01 and ESO 269-IG 022 NED02, and one very disturbed spiral galaxy, ESO 269-IG 023 NED01, hereafter AM 1256B. In addition, an isolated disc galaxy, ESO 269-IG 023 NED02/PGC 543979 ($\alpha = 12^h\,59^m\,00\overset{s}{.}6$ and $\delta = -43^h\,50^m\,23^s$ J2000), appears in the field of view of this system, about 30 arcsec to the south-east of the centre of AM 1256B. From our data, we obtained for this isolated galaxy a heliocentric velocity of 18 896 km s^{-1} indicating that it does not belong to this system, and it was incorrectly associated

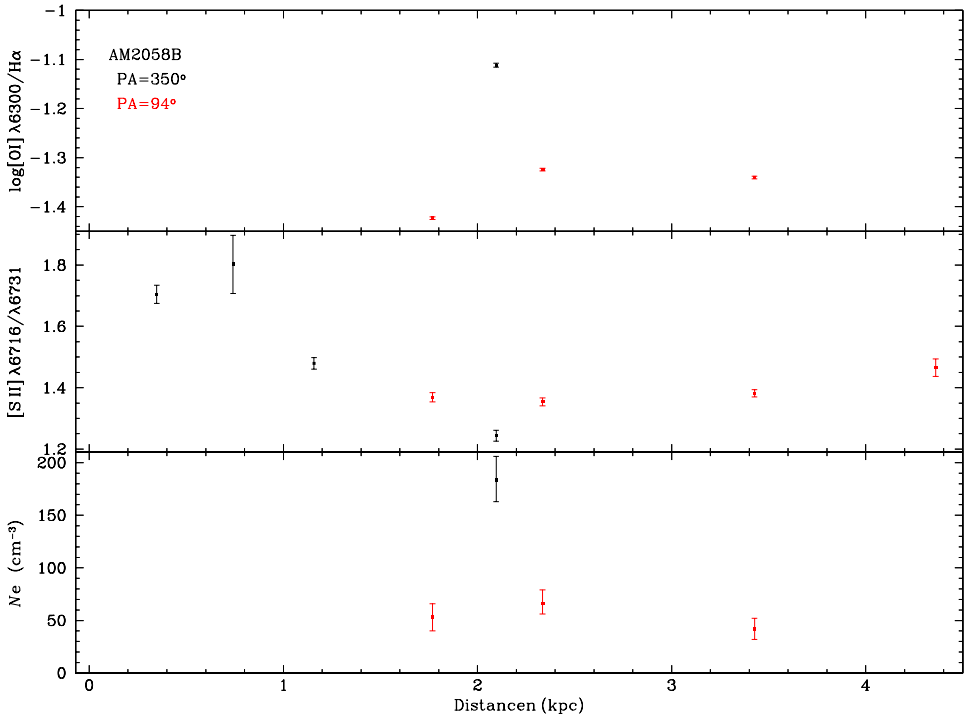

Figure 9. Same as Fig. 3, but for AM 2058B.

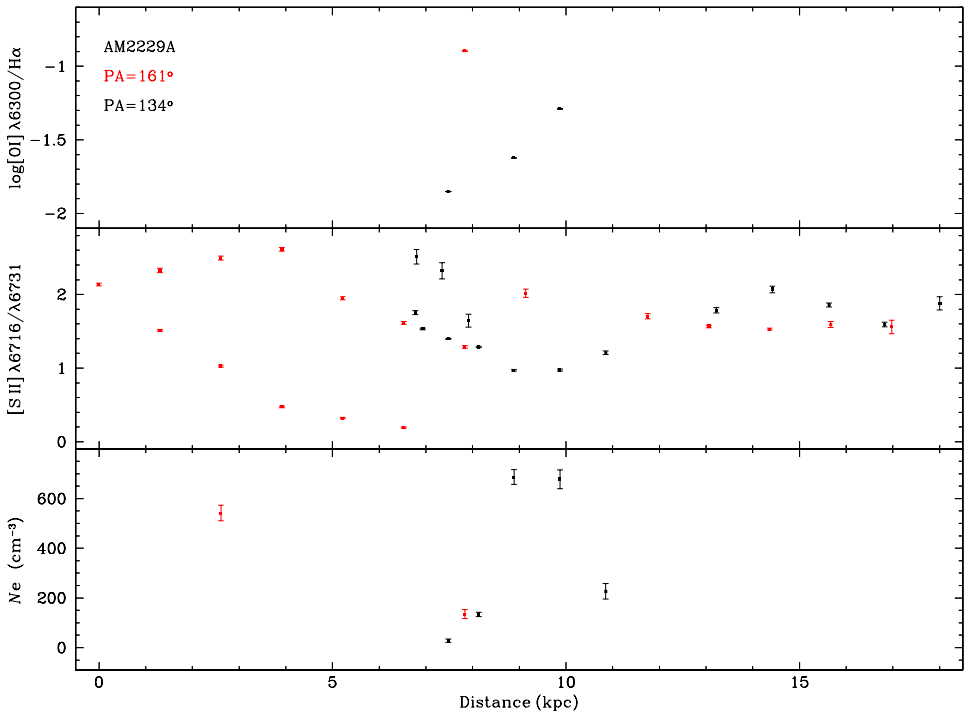

Figure 10. Same as Fig. 3, but for AM 2229A.

with AM 1256-433 by Donzelli & Pastoriza (1997), Ferreiro & Pastoriza (2004) and Ferreiro, Pastoriza & Rickes (2008). In Fig. 1, only AM 1256B and the isolated galaxy ESO 269-IG 023 NED02 are shown.

As can be seen in Fig. 7, some regions (for example at about 6 and 12 kpc from the centre of the galaxy) present unphysically large values of the [S II] λ6716/λ6731 ratio, above the theoretical value of 1.4, the value for the low-density limit according to the Osterbrock & Ferland (2006) curve for this relation. There could be some uncertainties associated with the measurements of these sulphur emission lines, due to the placement of the continuum and deblending of the lines, that might produce larger values of the [S II] ratio than the expected ones. Values of the [S II] ratio larger than the 1.4 upper limit were already observed in other studies using different kinds of instruments (e.g. Kennicutt, Keel & Blaha 1989; Zaritsky, Kennicutt & Huchra 1994; Lagos et al. 2009;

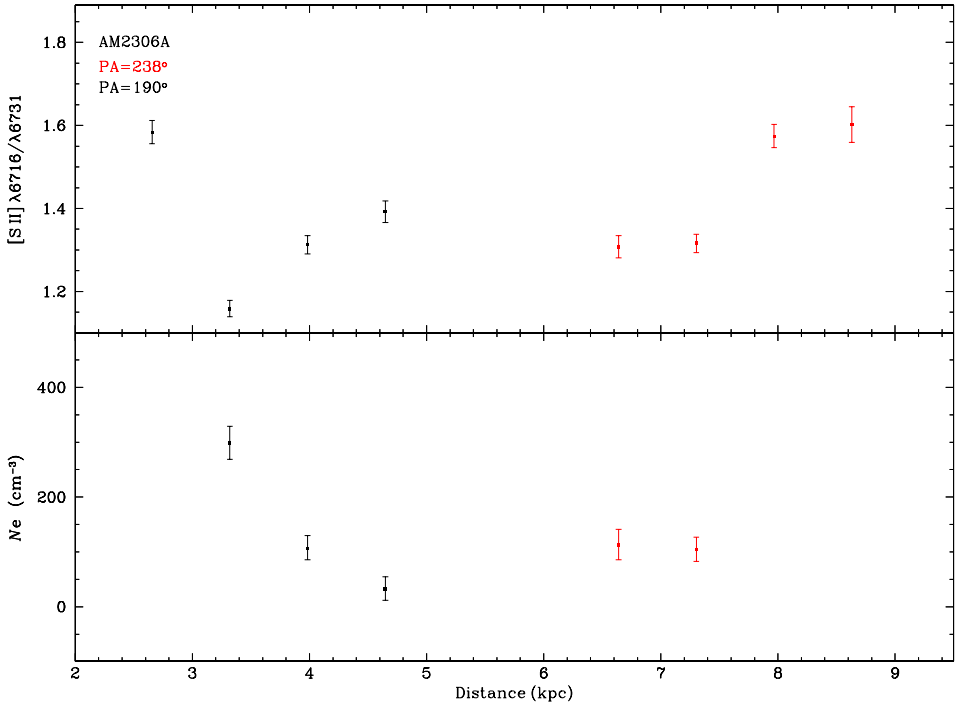

Figure 11. Same as Fig. 3, but for AM 2306A.

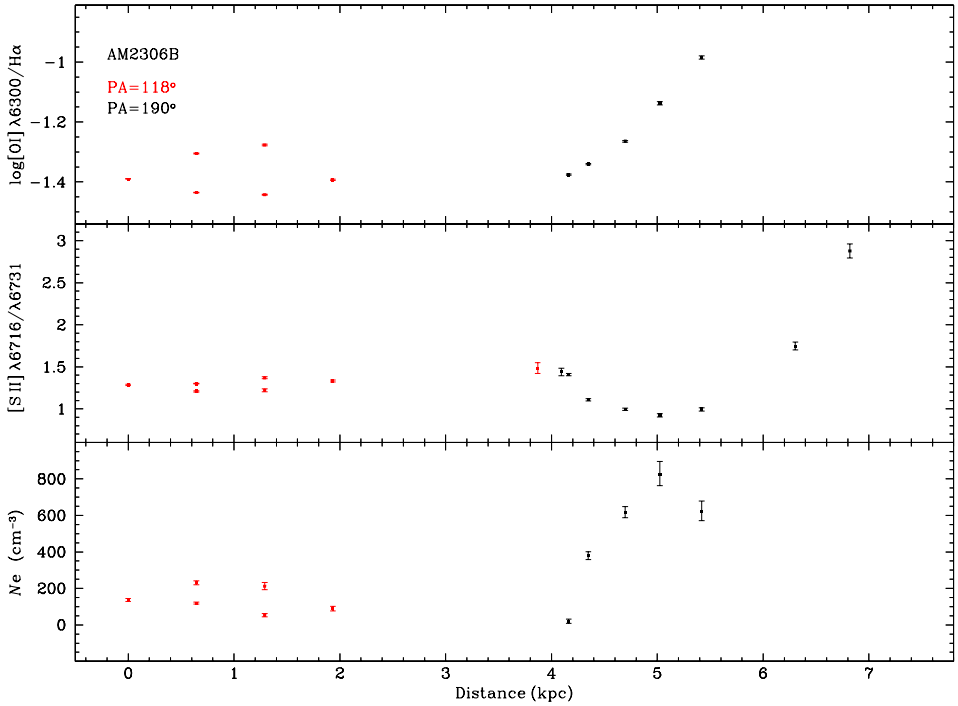

Figure 12. Same as Fig. 3, but for AM 2306B.

Relaño et al. 2010; López-Hernández et al. 2013). As pointed out by López-Hernández et al. (2013), the theoretical density determination also needs to be adjusted to the sulphur atomic data and deserves to be revisited. From a spatial distribution study of the electron density in a sample of H II regions in M33, these authors highlighted that when values of the λ6716/λ6731 ratio above the 1.4 limit are obtained, it is reasonable to assume that the electron densities are lower than 10 cm^{-3}. They also noted that a safe way to proceed is to take $N_e = 100\,cm^{-3}$, because even before reaching the 1.4 limit, the estimation of the electron density is very uncertain. A mean density of $N_e = 181 \pm 36\,cm^{-3}$ was derived for this galaxy. Again, the N_e increases towards the outskirts of this galaxy, corresponding to the end of the spiral arm at south-east.

4.4 AM 2058-381

This system of galaxies is a typical M51-type pair. It has a systemic velocity of $cz = 12\,286\,km\,s^{-1}$ (Donzelli & Pastoriza 1997) and

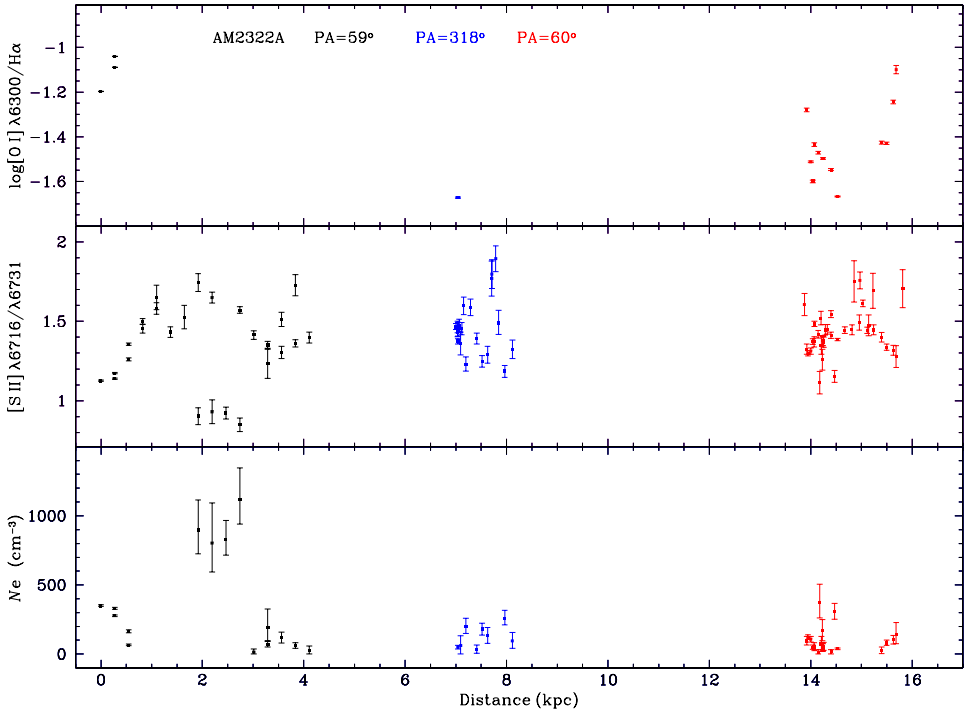

Figure 13. Same as Fig. 3, but for AM 2322A.

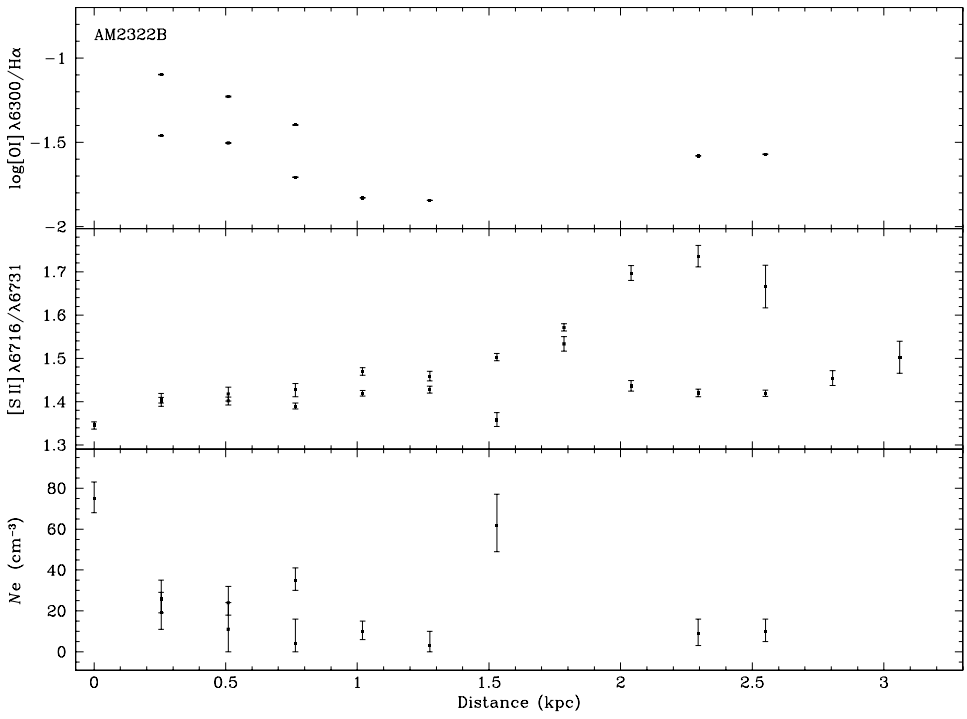

Figure 14. Same as Fig. 3, but for AM 2322B.

consists of a main galaxy with two spiral arms (hereafter AM 2058A) and a companion irregular galaxy (hereafter AM 2058B).

The electron densities obtained for AM 2058A have variations across the galaxy in the range of $N_e = 33-911\,cm^{-3}$, and these values are not dependent upon the position. Due to the small radius of AM 2058B, only a few apertures could be extracted for this galaxy. The electron densities (see Fig. 9) are relatively low, with a mean value of $N_e = 86 \pm 33\,cm^{-3}$, which is compatible with estimations for giant extragalactic H II regions (e.g. Castañeda et al. 1992).

4.5 AM 2229-735

This pair of galaxies consists of a main spiral galaxy strongly disturbed (hereafter AM 2229A) and a smaller disc galaxy that could

Table 3. [S II] ratio and electron density statistics.

	[S II] λ6716/λ6731						N_e (cm^{-3})					
Objects	N	Mean	Median	Max	Min	σ	N	Mean	Median	Max	Min	σ
AM 1054A	16	1.19	1.08	1.70	0.97	0.93	13	434	462	681	65	191
AM 1054B	3	0.86	0.85	0.92	0.79	0.07	3	1130	1082	1476	833	324
AM 1219A	29	1.12	1.06	1.77	0.86	0.23	26	532	518	1073	85	286
AM 1219B	5	0.70	0.82	0.92	0.23	0.27	4	1408	1294	2189	855	564
AM 1256B	43	1.48	1.42	2.08	0.99	0.27	22	181	317	626	7	168
AM 2058A	20	1.38	1.26	2.22	0.90	0.37	13	376	318	911	33	263
AM 2058B	8	1.47	1.42	1.80	1.24	0.19	4	86	60	184	42	66
AM 2229A	33	1.60	1.59	2.61	0.19	0.59	7	346	226	686	28	280
AM 2306A	8	1.41	1.44	1.60	1.16	0.16	5	131	107	298	32	99
AM 2306B	15	1.38	1.30	2.88	0.92	0.47	11	300	212	826	19	273
AM 2322A	81	1.41	1.42	1.89	0.85	0.20	41	200	103	1121	11	259
AM 2322B	23	1.47	1.43	1.74	1.35	0.10	12	24	15	75	3	23

be connected to the main one by a bridge. AM 2229A has a very massive nucleus of $M = 5 \times 10^8$ M$_\odot$ (Ferreiro et al. 2008) and very bright H II regions. Only the primary galaxy was observed.

Most of observed regions in AM 2229A present unphysically large values of the S II ratio according to the Osterbrock & Ferland (2006) curve for the relation between this ratio and the electron density. We derived a mean electron density of $N_e = 346 \pm 95$ cm^{-3}.

4.6 AM 2306-721

AM 2306-721 is a pair composed of a spiral galaxy with disturbed arms (hereafter AM 2306A) interacting with an irregular galaxy (hereafter AM 2306B). Both galaxies contain very luminous H II regions with Hα luminosity in the range of $8.30 \times 10^{39} \leq L$ (Hα) $\leq 1.32 \times 10^{42}$ erg s^{-1} and high SFR in the range of 0.07–10 M$_\odot$ yr^{-1}, as estimated from Hα images by Ferreiro et al. (2008).

The few measurements of electron densities provide values in the range of $N_e = 32-298$ cm^{-3} and $N_e = 19-826$ cm^{-3} for AM 2302A and AM 2306B, respectively. Although we do not have estimates of the electron density at the centre of the main galaxy, the spatial profile seems to indicate an increase in the N_e towards the centre of the galaxy, which could be a consequence of gas inflow. Again, in the secondary galaxy, the electron density smoothly increases from about 4 kpc towards the outer regions of the galaxy to the end of the spiral arm at the south-east.

4.7 AM 2322-821

AM 2322-821 is composed of an SA(r)c galaxy with disturbed arms (hereafter AM 2322A) in interaction with an irregular galaxy (hereafter AM 2322B). Both galaxies contain very luminous H II regions with $2.53 \times 10^{39} \leq L$ (Hα) $\leq 1.45 \times 10^{41}$ erg s^{-1} and SFR from 0.02 to 1.15 M$_\odot$ yr^{-1} (Ferreiro et al. 2008).

The distribution of electron temperatures exhibits variations of very low amplitude across the radius of AM 2322A. One region (at about 2 kpc from the centre of the galaxy) has four values of densities systematically higher than the other apertures along the radius of galaxy. This region is marked in Fig. 15. In this region, the values of densities are in the range of $N_e = 803-1121$ cm^{-3}. We found a mean electron density of $N_e = 200 \pm 12$ cm^{-3}. AM 2322B presents a relatively homogeneous electron density distribution, with a mean density of $N_e = 24 \pm 4.8$ cm^{-3}. This is the galaxy with the lowest density in our sample.

5 DISCUSSION

To verify if there are differences between the N_e values observed in the H II regions of our sample and those obtained in isolated galaxies, we have calculated the electron densities from published measurements of the [S II] line ratio for disc H II regions in the isolated galaxies M101, NGC 1232, NGC 1365, NGC 2903, NGC 2997 and NGC 5236 and compared these values with our results. The data of these objects were taken from Kennicutt, Bresolin & Garnett (2003) for M101 and from Bresolin et al. (2005) for the other galaxies. The same atomic parameters and electron temperature adopted for our determinations were used. The spatial profiles of the [S II] λ6716/λ6731 ratio and the electron densities derived for some H II regions in the isolated galaxies are shown in Fig. 16.

As can be seen in this figure, the estimated electron densities are relatively homogeneous along the radius of each isolated galaxy. The derived mean electron densities are in the range of $N_e = 40-137$ cm^{-3}. Only one high value of $N_e \approx 900$ cm^{-3} is derived in the central region of NGC 5236. It is a metal-rich H II region, with a low electron temperature of T_e(O III) $= 4000 \pm 2000$ K and an oxygen abundance of 12+log(O/H) ≈ 8.9 dex as derived by Bresolin et al. (2005). This high value can be caused by mass-loss and strong stellar winds from embedded Wolf–Rayet stars, which are common in metal-rich environments (e.g. Schaerer et al. 2000; Bresolin & Kennicutt 2002; Pindao et al. 2002). If the adopted electron temperature is T_e(O III) $= 4000$ K, an estimation of $N_e \approx 623$ cm^{-3} is obtained. This value is about 30 per cent lower than the one obtained assuming an electron temperature of T_e(O III)=10 000 K. Then, even though the dependence of the N_e on the electron temperature is weak, it could have an important effect when temperature fluctuations of high amplitude were observed in H II regions.

The values of the electron density obtained from our sample of interacting galaxies are systematically higher than those derived for the isolated ones. The mean electron density values derived by us for the interacting galaxies in our sample are in the range of $N_e = 24$–532 cm^{-3}, which also show higher values than for isolated galaxies. Newman et al. (2012), for the clumpy star-forming galaxy ZC 406690, also obtained high electron density values ($N_e = 300$–1800 cm^{-3}). Moreover, several of our interacting galaxies (AM 2306B, AM 1219A and AM 1256B) show a slight increment of the N_e in the outer parts of the galaxy, opposite of what is observed in the isolated galaxies, where the electron density is homogeneous along the radius. The high electron density values found in the outlying parts for the majority of the objects of

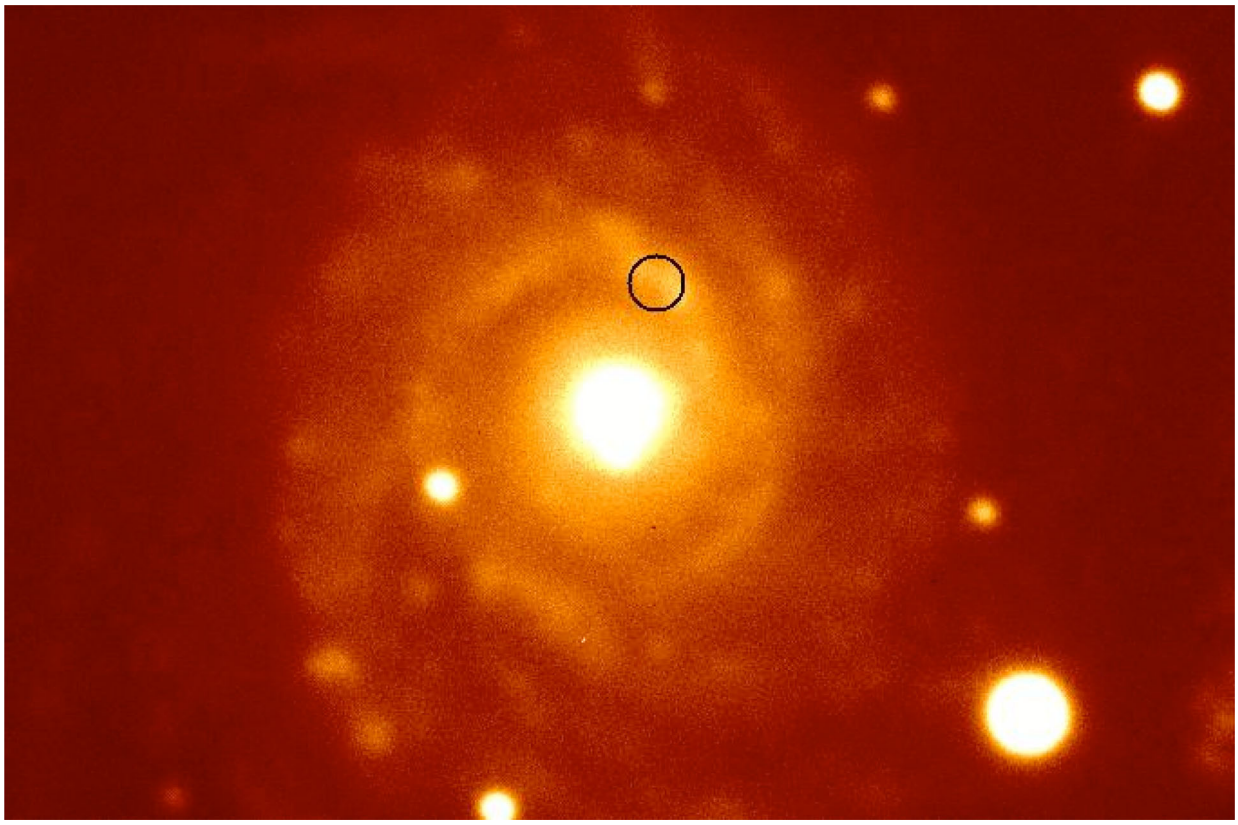

Figure 15. Image of AM 2322A with the region of high density (see the text) marked with a circle.

our sample would be due to zones of induced star formation by a direct cloud–cloud interaction (for a review see Bournaud 2011). In these regions, turbulent flows can locally compress the gas, forming overdensities that subsequently cool and collapse into star-forming clouds (Elmegreen 2002; Duc et al. 2013). Although we do not have estimates of the electron density at the centre of AM 2306A, the spatial profile seems to indicate an increase of N_e towards the centre of the galaxy, which could be due to inflowing gas. However, in only a few regions in this galaxy it was possible to estimate N_e; therefore, this is a marginal conclusion.

It is worth mentioning that H II regions seemed to be inhomogeneous, and the zones where most of the emission from the ionized gas is originated only occupy a small fraction of the total volume (i.e. small filling factor). Hence, our electron density values derived from the [S II] emission lines are representative of a fraction of the total volume of the H II region (referred to as in situ electron densities). According to Giammanco et al. (2004), these inhomogeneities, if optically thick, can modify the determinations of electron temperatures and densities, ionization parameters and abundances. Copetti et al. (2000) presented a study on internal variation of the electron density in a sample of spatially resolved galactic H II regions of different sizes and evolutionary stages. These authors found that the electron density within H II regions (e.g. S 307) can range from about 30 to 600 cm^{-3}, and a filling factor of the order of 0.1 is compatible with their data. Therefore, the estimated electron densities could be about 10 per cent of the in situ values sampled by the sulphur line ratio.

An important issue is to study the origin of the high electron density values found in the H II regions of our sample. The presence of gas shock excitation in interacting galaxies is very important not only because they affect quantities derived from spectroscopy, but also because they act as a mechanism for dissipating the kinetic energy and the angular momentum of the infalling gas in merging systems, as discussed by Rich et al. (2011). The gas shock also increases the density due to the compression of the interstellar material. To analyse if the presence of shock-excited gas produces the high electron density values, the diagnostic diagram [O III] λ5007/Hβ versus [O I] λ6300/Hα proposed by Baldwin, Phillips & Terlevich (1981) and Veilleux & Osterbrock (1987), and used to separate objects ionized by stars, by shocks and/or active nuclei (AGN), was considered.

In Fig. 17, the diagnostic diagram containing the data of the H II regions studied by us is shown. The galaxy nucleus data are not shown in this diagram. We also show in this plot the line proposed by Kewley et al. (2006) to separate objects with distinct ionizing sources: shock gas and massive star excitations. We can see that all the H II regions in AM 1054A, AM 2058B, AM 2306B, and some regions in AM 2322A (three apertures) and AM 2322B (one aperture) occupy the area where objects with shock as the main ionizing source are located. The number of objects represented in Fig. 17 differs from those in the profile figures (Figs 3–14) because the [O III] λ5007/Hβ ratio could not be measured for all apertures. From the comparison of the spatial profiles of the electron density and the logarithm of [O I] λ6300/Hα in the AM 1054A, AM 2058B and AM 2306B galaxies (Figs 3, 9 and 12, respectively), we can note the following.

(i) AM 1054A: all regions of this galaxy have gas shock excitation and the values of electron density are relatively high.

(ii) AM 2058B: it is a small galaxy and only a few apertures could be extracted. As can be seen in Fig. 17, all four disc H II regions of this galaxy have gas shock excitation, and from Fig. 9,

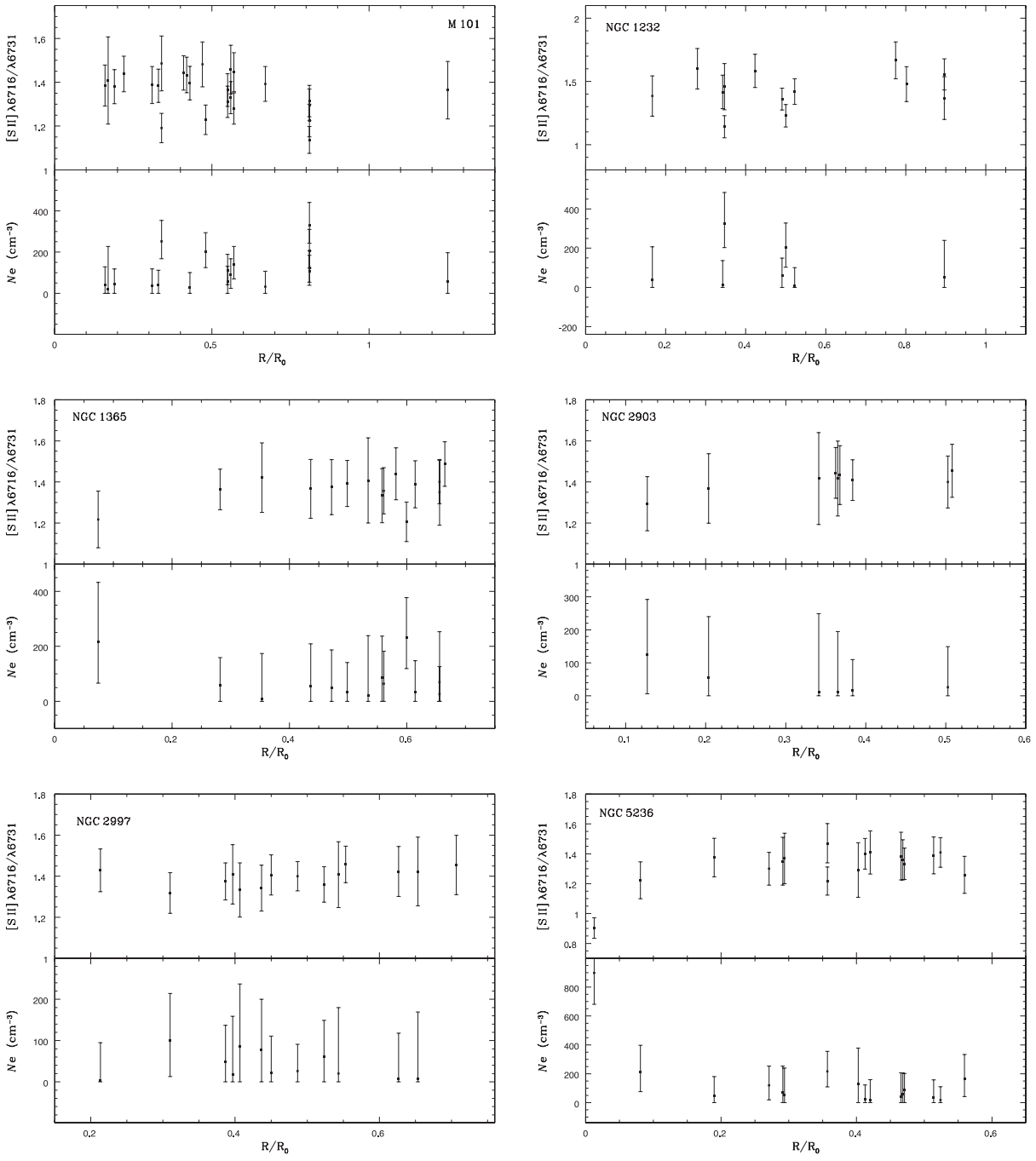

Figure 16. Profiles of the electron density as a function of R/R_0, where R_0 is the galactocentric distance deprojected for the isolated galaxies M101, NGC 1232, NGC 1365, NGC 2903, NGC 2997 and NGC 5236.

we can note that these regions present low electron density values ($<200\,\mathrm{cm}^{-3}$).

(iii) AM 2306B: the regions with highest [O I] λ6300/Hα and N_e values ($\approx 700\,\mathrm{cm}^{-3}$) lie in the outskirts of galaxy. As can be seen in Fig. 12, it seems to be a trend in this object: from about 4 kpc both the N_e and the [O I]/Hα ratio increase to the outer parts of the galaxy; in the inner part (up to 2 kpc), the profiles of these two quantities are almost flat showing low values.

It is essential to find out the cause of the high electron density values associated with the shock excitation region in interacting galaxies to understand how the flux gas works in them. High-velocity gas motions can destroy molecular clouds and quench star formation (Tubbs 1982). To investigate if the high electron density values found in our sample are associated with the presence of excitation by gas shock, we plotted in Fig. 18 the N_e versus the logarithm of the observed [O I] λ6300/Hα emission line ratio. Objects with distinct gas excitation source, according to Fig. 17, are indicated by different symbols. No correlation is obtained between the presence of shocks and electron densities. The highest electron density values found in our sample do not belong to objects with gas shock excitation. Therefore, the high electron density values found in the H II regions of our sample do not seem to be caused by the presence of gas shock excitation. However, a deeper analysis such as

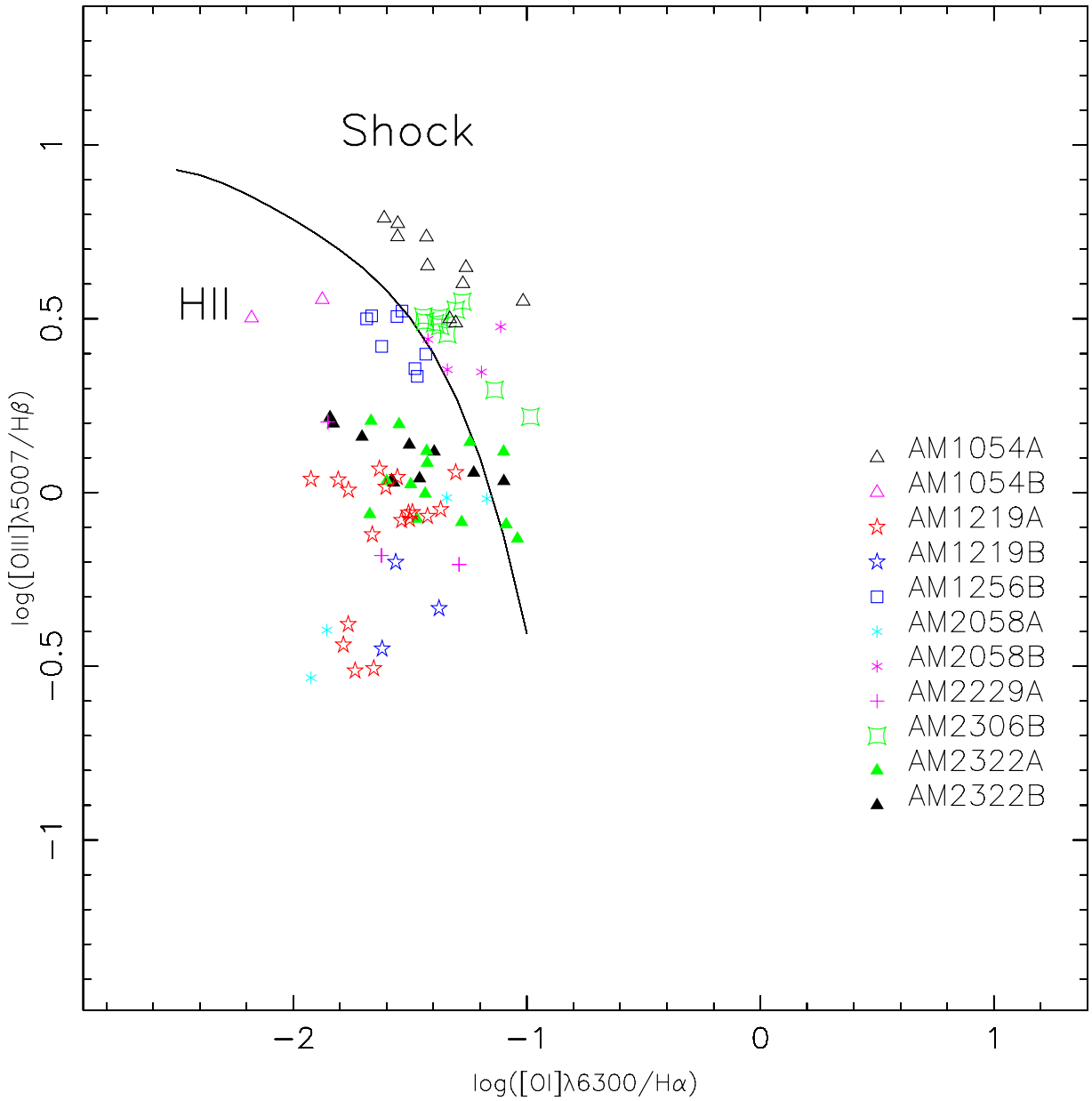

Figure 17. Diagnostic diagram of [O III] λ5007/Hβ versus [O I] λ6300/Hα. The black solid line from Kewley et al. (2006) separates the objects ionized by massive stars from the ones containing active nuclei and/or shock-excited gas. The data for distinct galaxies are marked by different symbols as indicated. The typical error bar (not shown) of the emission line ratios is about 10 per cent.

investigating the presence of a correlation between the velocity dispersion of some emission line and its intensity (e.g. Storchi-Bergmann et al. 2007) or the implications of multiple kinematical components in the emission line profiles on the derived properties (Amorín et al. 2012; Hägele et al. 2012, 2013) is necessary to confirm our result. Interestingly, the objects with the highest electron density values present the smallest [O I] λ6300/Hα line intensity ratios.

6 CONCLUSIONS

An observational study of the effects of the interaction on the electron densities from the H II regions along the radius of a sample of interacting galaxies is performed. The data consist of long-slit spectra of high signal-to-noise ratio in the 4390–7250 Å obtained with the GMOS-S. The electron density was determined using the ratio of lines [S II] λ6716/λ6731. The main findings are the following.

(i) The electron density estimates obtained for some H II regions of our sample of interacting galaxies are systematically higher than those derived for isolated galaxies in the literature. The mean electron density values of interacting galaxies are in the range of $N_e = 24-532\,cm^{-3}$, while those obtained for isolated galaxies are in the range of $N_e = 40-137\,cm^{-3}$.

(ii) Some interacting galaxies: AM 2306B, AM 1219A and AM 1256B show an increment of N_e towards the outskirts of each system. This kind of relation is not observed in isolated galaxies, where the electron density profile is rather flat along the radius of each galaxy.

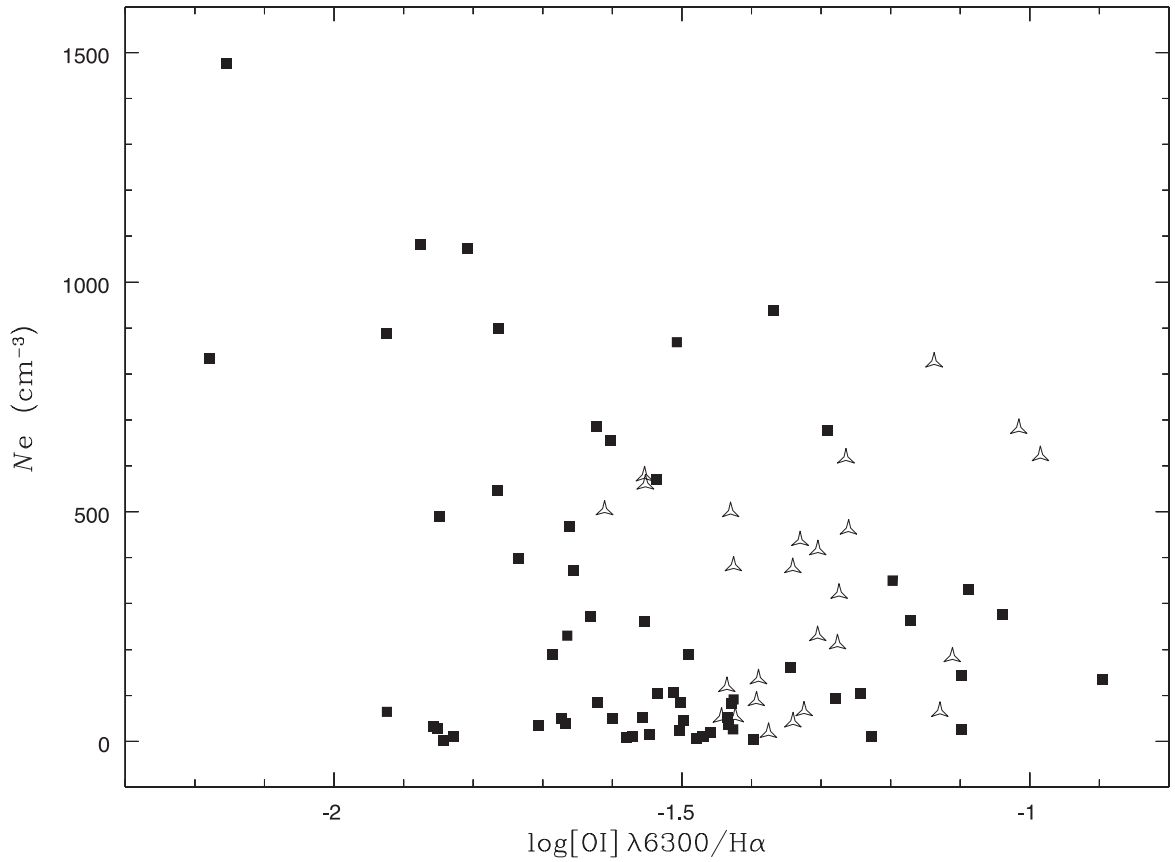

Figure 18. Electron density values N_e derived for our sample versus the observed [O I] λ6300/Hα ratio. The squares represent regions ionized by massive stars while the triangles represent those with gas shock excitation, according to the diagnostic diagram presented in Fig. 17.

(iii) The galaxies where the mechanism of gas shock excitation is present in almost all the H II regions are AM 1054A, AM 2058B and AM 2306B. For the remaining galaxies, only few H II regions have emission lines excited by shocks, such as in AM 2322B (one point) and AM 2322A (four points). It is noteworthy that only in three of all objects analysed here, the main excitation mechanism for all of their H II regions is shocks.

(iv) No correlation is obtained between the presence of shocks and electron densities. Indeed, the highest electron density values found in our sample do not belong to the objects with gas shock excitation. Therefore, the high electron density values found in the H II regions of our sample do not seem to be caused by the presence of gas shock excitation.

ACKNOWLEDGEMENTS

This work is based on observations obtained at the Gemini Observatory, which is operated by the Association of Universities for Research in Astronomy, Inc., under cooperative agreement with the NSF on behalf of the Gemini partnership: the National Science Foundation (United States), the Science and Technology Facilities Council (United Kingdom), the National Research Council (Canada), CONICYT (Chile), the Australian Research Council (Australia), Ministério da Ciencia e Tecnologia (Brazil) and SECYT (Argentina).

ACK, OLD and DAR acknowledge the support of FAPESP, process 2010/01490-3, 2009/14787-7 and 2011/08202-6, respectively.

We also thank Ms. Alene Alder-Rangel for editing the English in this manuscript.

REFERENCES

Amorín R., Vílchez J. M., Hägele G. F., Firpo V., Pérez-Montero E., Papaderos P., 2012, ApJ, 754, L22
Baldwin J. A., Phillips M. M., Terlevich R., 1981, PASP, 93, 5
Bournaud F., 2011, EAS Publ. Ser., 51, 107
Bowen I. S., 1960, ApJ, 132, 1
Bresolin F., Kennicutt R. C., 2002, ApJ, 572, 838
Bresolin F., Schaerer D., González Delgado R. M., Stasińska G., 2005, A&A, 441, 981
Castañeda H. O., Vílchez J. M., Copetti M. V. F., 1992, A&A, 260, 370
Copetti M. V. F., Writzl B. C., 2002, A&A, 382, 282
Copetti M. V. F., Mallmann J. A. H., Schmidt A. A., Castañeda H. O., 2000, A&A, 357, 621
de Vaucouleurs G., de Vaucouleurs A., Corwin H. G., Jr, Buta R. J., Paturel G., Fouqué P., 1991, Third Reference Catalogue of Bright Galaxies Sky and Telescope. Springer, New York, p. 621
Donzelli C. J., Pastoriza M. G., 1997, ApJS, 111, 181
Dopita M. A., Kewley L. J., Heisler C. A., Sutherland R. S., 2000, ApJ., 542, 224
Dors O. L., Jr, Krabbe A., Hägele G. F., Pérez-Montero E., 2011, MNRAS, 415, 3616
Duc P.-A., Belles P.-E., Brinks E., Bournaud F., 2013, in Wong T., Ott J., eds, Proc. IAU Symp. 292, Molecular Gas, Dust, and Star Formation. Cambridge Univ. Press, Cambridge, p. 323
Elmegreen B. G., 2002, ApJ, 577, 206
Ferreiro D. L., Pastoriza M. G., 2004, A&A, 428, 837
Ferreiro D. L., Pastoriza M. G., Rickes M., 2008, A&A, 481, 645
Giammanco C., Beckman J. E., Zurita A., Relaño M., 2004, A&A, 424, 877
Hägele G. F., Firpo V., Bosch G., Díaz Á. I., Morrell N., 2012, MNRAS, 422, 3475

Hägele G. F., Díaz Á. I., Terlevich R., Terlevich E., Bosch G. L., Cardaci M. V., 2013, MNRAS, 432, 810
Huchra J. P. et al., 2012, ApJS, 199, 26
Jones D. H. et al., 2009, MNRAS, 399, 683
Keenan F. P., Hibbert A., Ojha P. C., Collon E. S., 1993, Phys. Scr. A., 47, 48
Kennicutt R. C., 1984, ApJ, 287, 116
Kennicutt R. C., Jr, Keel W. C., Blaha C. A., 1989, AJ, 97, 1022
Kennicutt R. C., Bresolin F., Garnett D. R., 2003, ApJ, 591, 801
Kewley L. J., Dopita M. A., 2002, ApJS, 145, 35
Kewley L. J., Groves B., Kauffmann G., Heckman T., 2006, MNRAS, 372, 961
Kewley L. J., Rupke D., Jabran Hahid H., Geller M. J., Barton E. J., 2010, ApJ, 721, L48
Krabbe A. C., Pastoriza M. G., Winge C., Rodrigues I., Ferreiro D. L., 2008, MNRAS, 389, 1593
Krabbe A. C., Pastoriza M. G., Winge C., Rodrigues I., Dors O. L., Ferreiro D. L., 2011, MNRAS, 416, 38
Lagos P., Telles E., Muñoz-Tuñón C., Carrasco E. R., Cuisinier F., Tenorio-Tagle G., 2009, AJ, 137, 5068
Lauberts A., 1982, Garching: European Southern Observatory (ESO)
Lauberts A., Valentijn E. A., 1989, The Messenger, 56, 31
López-Hernández J., Terlevich E., Terlevich R., Rosa-González D., Díaz Á., García-Benito R., Vílchez J., Hägele G., 2013, MNRAS, 430, 472
Newman S. F. et al., 2012, ApJ, 752, 111
O'Dell C. R., Castañeda H. O., 1984, ApJ, 283, 158
Oey M. S., Kennicutt R. C., 1993, ApJ, 411, 137
Osterbrock D. E., Ferland G. J., 2006, Astrophysics of Gaseous Nebulae and Active Galactic Nuclei, 2nd edn. University Science Books, Mill Valley, CA
Paturel G., Petit C., Prugniel P., Theureau G., Rousseau J., Brouty M., Dubois P., Cambrésy L., 2003, A&A, 412, 45
Pindao M., Schaerer D., González Delgado R. M., Stasińska G., 2002, A&A, 394, 443
Puech M., Flores H., Hammer F., Lehnert M. D., 2006, A&A, 455, 131, 134
Ramsbottom C. A., Bell K. L., Stafford R. P., 1996, At. Data Nucl. Data Tables, 63, 57
Relaño M., Monreal-Ibero A., Vílchez J. M., Kennicutt R. C., 2010, MNRAS, 402, 1635
Rich J. A., Kelley L. J., Dopita M. A., 2011, ApJ, 734, 87
Rich J. A., Torrey T., Kelley L. J., Dopita M. A., Rupke D. S. N., 2012, ApJ, 753, 5
Rupke D. S. N., Kewley L. J., Chien L.-H., 2010, ApJ, 710, L156
Schaerer D., Guseva N. G., Izotov Y. I., Thuan T. X., 2000, A&A, 362, 53
Scudder J. M., Ellison S. L., Torrey P., Patton D. R., Mendel J. T., 2012, MNRAS, 426, 549
Sekiguchi K., Wolstencroft R. D., 1993, MNRAS, 263, 349
Soto K. T., Martin C. L., 2012, ApJS, 203, 3
Soto K. T., Martin C. L., Prescott M. K. M., Armus L., 2012, ApJS, 757, 86
Stanghellini L., Kaler J. B., 1989, ApJ, 343, 811
Storchi-Bergmann T., Dors O. L., Jr, Riffel R. A., Fathi K., Axon D. J., Robinson A., Marconi A., Östlin G., 2007, ApJ, 670, 959
Tubbs A. D., 1982, ApJ, 255, 458
Veilleux S., Osterbrock D. E., 1987, ApJS, 63, 295
Veilleux S., Cecil G., Bland-Hawthorn J., 2005, ARA&A, 43, 76
Verner D. A., Verner E. M., Ferland G. J., 1987, At. Data Nucl. Data Tables, 1, 64
Weilbacher P. M., Duc P.-A., Fritze v. Alvensleben U., Martin P., Fricke K. J., 2000, A&A, 358, 819
Zaritsky D., Kennicutt R. C., Jr, Huchra J. P., 1994, ApJ, 420, 87

This paper has been typeset from a TEX/LATEX file prepared by the author.